J|A|C|S
ARTICLES

Published on Web 04/22/2009

Crystal Structures of Cyclohexanone Monooxygenase Reveal Complex Domain Movements and a Sliding Cofactor

I. Ahmad Mirza,[†] Brahm J. Yachnin,[†] Shaozhao Wang,[‡] Stephan Grosse,[‡] Hélène Bergeron,[‡] Akihiro Imura,[||] Hiroaki Iwaki,[§] Yoshie Hasegawa,[§] Peter C. K. Lau,*[,‡] and Albert M. Berghuis*[,†]

Departments of Biochemistry and Microbiology & Immunology, McGill University, 3649 Prom Sir William Osler, Bellini Pavilion, Room 466, Montreal, QC, Canada H3G 0B1, Biotechnology Research Institute, National Research Council Canada, 6100 Royalmount Avenue, Montreal, QC, Canada H4P 2R2, Department of Life Science & Biotechnology and ORDIST, Kansai University, Suita, Osaka, 564-8680, Japan, and Process Technology Research Laboratories, Daiichi Sankyo Co. Ltd, Kasai R&D Center, 1-16-13, Kitakasai Edogawa-ku, Tokyo 134-8630, Japan

Received February 10, 2009; E-mail: peter.lau@cnrc-nrc.gc.ca; albert.berghuis@mcgill.ca

Abstract: Cyclohexanone monooxygenase (CHMO) is a flavoprotein that carries out the archetypical Baeyer−Villiger oxidation of a variety of cyclic ketones into lactones. Using NADPH and O_2 as cosubstrates, the enzyme inserts one atom of oxygen into the substrate in a complex catalytic mechanism that involves the formation of a flavin-peroxide and Criegee intermediate. We present here the atomic structures of CHMO from an environmental *Rhodococcus* strain bound with FAD and $NADP^+$ in two distinct states, to resolutions of 2.3 and 2.2 Å. The two conformations reveal domain shifts around multiple linkers and loop movements, involving conserved arginine 329 and tryptophan 492, which effect a translation of the nicotinamide resulting in a sliding cofactor. Consequently, the cofactor is ideally situated and subsequently repositioned during the catalytic cycle to first reduce the flavin and later stabilize formation of the Criegee intermediate. Concurrent movements of a loop adjacent to the active site demonstrate how this protein can effect large changes in the size and shape of the substrate binding pocket to accommodate a diverse range of substrates. Finally, the previously identified BVMO signature sequence is highlighted for its role in coordinating domain movements. Taken together, these structures provide mechanistic insights into CHMO-catalyzed Baeyer−Villiger oxidation.

Introduction

For reasons of exquisite chemo-, regio-, and enantioselectivity, the enzyme cyclohexanone monooxygenase (CHMO), produced by *Acinetobacter* sp. NCIMB 9871, has been the subject of study for over 30 years.[1−4] A member of the Baeyer−Villiger monooxygenase (BVMO) family, and in the superfamily of flavin-containing monooxygenases (FMO^5), it is highly valued for its ability to produce lactones and other important chiral building blocks while producing only water as a clean byproduct.[6,7] Current increasing interests in CHMO are specifically focused on possible use in asymmetric synthesis for the pharmaceutical industry, as it avoids hazardous reagents like organic peracids, chlorinated solvents, and metals that are otherwise used in chemical Baeyer−Villiger reactions.[8−12]

The mechanism of CHMO-catalyzed oxidation of cyclohexanone, and BVMO-catalyzed reactions in general, has been shown by kinetic and spectroscopic data to proceed in a manner very similar to the century-old chemical Baeyer−Villiger reactions.[12−15] In this chemical reaction, addition of an oxidant, such as *m*-chloroperoxybenzoic acid, to the carbonyl group of a ketone creates a tetrahedral intermediate that undergoes "Criegee" rearrangement to yield the corresponding ester or lactone. With BVMOs (Scheme 1), the tightly bound FAD molecule is reduced by NADPH. The reduced flavin then reacts

[†] McGill University.
[‡] National Research Council Canada.
[§] Kansai University.
[||] Daiichi Sankyo Co. Ltd.

(1) Donoghue, N. A.; Trudgill, P. W. *Eur. J. Biochem.* **1975**, *60*, 1–7.
(2) Stewart, J. D. *Curr. Org. Chem.* **1998**, 192–216.
(3) Schwab, J. M.; Li, W.; Thomas, L. P. *J. Am. Chem. Soc.* **1983**, *105*, 4800–4808.
(4) Gibson, M.; Nur-e-alam, M.; Lipata, F.; Oliveira, M. A.; Rohr, J. *J. Am. Chem. Soc.* **2005**, *127*, 17594–17595.
(5) van Berkel, W. J. H.; Kamerbeek, N. M.; Fraaije, M. W. *J. Biotechnol.* **2006**, *124*, 670–689.
(6) Stewart, J. D.; Reed, K. W.; Martinez, C. A.; Zhu, J.; Chen, G.; Kayser, M. M. *J. Am. Chem. Soc.* **1998**, *120*, 3541–3548.
(7) ten Brink, G. J.; Arends, I. W.; Sheldon, R. A. *Chem. Rev.* **2004**, *104*, 4105–4124.
(8) Alphand, V.; Carrea, G.; Wohlgemuth, R.; Furstoss, R. *Trends Biotechnol.* **2003**, *21*, 318–323.
(9) Constable, D. J. C.; Dunn, P. J.; Hayler, J. D.; Humphrey, G. R. *Green Chem.* **2007**, *9*, 411–420.
(10) Kamerbeek, N. M.; Janssen, D. B.; van Berkel, W. J. H.; Fraaije, M. W. *Adv. Synth. Catal.* **2003**, *345*, 667–678.
(11) Mihovilovic, M. D.; Mueller, B.; Stanetty, P. *Eur. J. Org. Chem.* **2002**, 3711–3730.
(12) Kayser, M. M. *Tetrahedron: Asymmetry* **2009**, 947–974.
(13) Renz, M.; Meunier, B. *Eur. J. Org. Chem.* **1999**, 737–750.
(14) Ryerson, C. C.; Ballou, D. P.; Walsh, C. T. *Biochemistry* **1982**, *21*, 2644–2655.
(15) Sheng, D.; Ballou, D. P.; Massey, V. *Biochemistry* **2001**, *40*, 11156–11167.

 10.1021/ja9010578 CCC: $40.75

Scheme 1. Reaction Mechanism of CHMO[a]

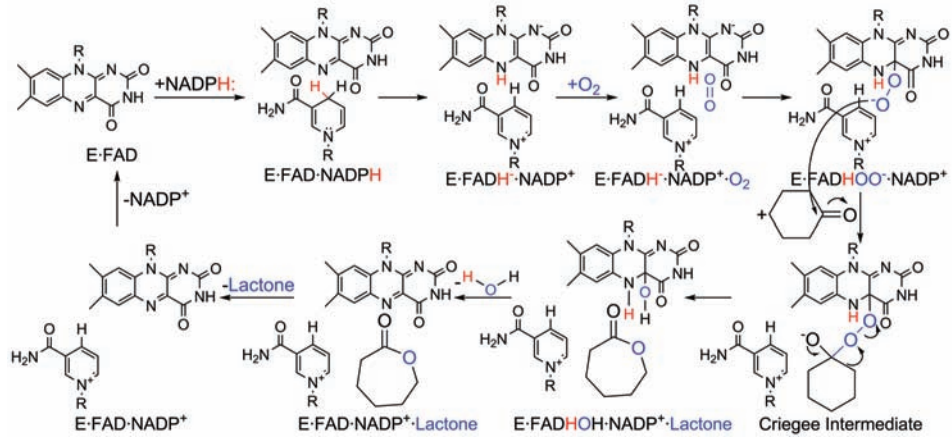

[a] The atoms of the NADPH hydride and molecular oxygen are tracked throughout the reaction mechanism using red and blue, respectively.

with molecular oxygen to form a C4A-peroxyflavin intermediate ($E{\cdot}FADHOO^{-}{\cdot}NADP^{+}$). This peroxyflavin intermediate plays the same role as the peracid in the conventional Baeyer−Villiger oxidation reaction,[15] acting as the nucleophile in the nucleophilic attack of the carbonyl carbon of the ketone substrate. This produces the tetrahedral Criegee intermediate that subsequently rearranges to give the C4a-hydroxyflavin and ε-caprolactone, a ring-expanded product.[16] A molecule of water is spontaneously eliminated from the hydroxyflavin to regenerate the oxidized FAD. It is noteworthy that in this reaction, the NADPH, which is the first species to bind to the enzyme and react with the flavin, is held in the active site in the $NADP^{+}$ form until the last step of the reaction cycle.

Even though the CHMO of *Acinetobacter* sp. NCIMB 9871 has been the most extensively studied among numerous BVMOs, to date there is no structural model available for this enzyme. The only crystal structure that is currently available for a BVMO enzyme is that of phenylacetone monooxygenase (PAMO), which comes from a moderate thermophilic microorganism, *Thermobifida fusca*.[17] The structure of PAMO was solved with bound FAD in the absence of NADP cofactor and/or substrates (analogues) and suggested a multidomain architecture resembling that of the disulfide oxidoreductases. It allowed for the identification of the active site and a number of residues critical for catalysis but also highlighted the functional complexity of BVMOs. Specifically, the authors speculated on the nature of the conformational changes that must occur to enable the sequential binding of the different substrates to the enzyme and the formation of several distinct catalytic intermediates that are consistent with spectroscopic data.[15,17]

Here, we present multiple crystal structures of CHMO from *Rhodococcus* sp. strain HI-31 in complex with FAD and $NADP^{+}$. The two structures reveal the nature of conformational changes required for catalysis and clarify how the NADP cofactor can perform different roles in the reaction mechanism. Our results also provide insight into the structural basis for CHMO's ability to accommodate a diverse range of substrates. Finally, the structural data rationalize the role of the previously identified BVMO signature sequence which has thus far remained enigmatic.[17]

Materials and Methods

For a complete description of the cloning of the *chnB1* gene from *Rhodococcus* sp. strain HI-31, and overexpression, purification, mutagenesis of the CHMO enzyme, refer to the Supporting Information (SI).

Substrate Profiling. Standards of racemic lactones were preparaed by oxidation of the cyclic ketones with *m*-CPBA according to literature reports of Baeyer−Villiger oxidation.[6] All ketone substrates used in this study were purchased from Aldrich Chemical Co. and used without further purification.

The ability of CHMO to transform cyclic ketones besides cyclohexanone was investigated using whole cells of *Escherichia coli* BL21(DE3)pSDRmchnB1. Conditions of whole-cell biotransformation were carried out as previously described.[18,19] Reaction samples were extracted with ethyl acetate, dried with $MgSO_4$, and analyzed by GC/MS, using a Hewlett-Packard HP6890 series gas chromatograph (GC system) connected to an HP5971 mass-selective detector (Hewlett-Packard) and a DB-1 capillary column (J&W Scientific, Folsom, CA). Chiral capillary-column GC was performed on a Perkin-Elmer Sigma 2000 gas chromatograph, employing a 0.25 mm × 30 m (0.25-μm film) β-Dex 225 column (Supelco Inc.). Peaks were identified by comparison of their retention times and their mass spectra with those of authentic standards. ^{1}H and ^{13}C nuclear magnetic resonance (NMR) analyses were performed on a Bruker Avance-500 spectrometer, and the spectra were recorded in a $CDCl_3$ solution at room temperature.

Crystallization and Data Collection. Two different crystal forms of the enzyme were obtained by either hanging drop or sitting drop vapor diffusion methods. Crystals were grown in 4-μL drops containing equal volumes of concentrated (10 mg/mL) protein solution mixed in a 5 M excess of $NADP^{+}$ (Sigma) with well solution. For crystal form I, the well solution contained 0.2 M sodium acetate trihydrate, 0.1 M sodium cacodylate pH 6.5, and 30% PEG 8000. For crystal form II, the well solution consisted of 0.2 M magnesium acetate tetrahydrate, 0.1 M sodium cacodylate pH 6.5, and 20% PEG 8000 (Nextal). Diffraction data for $CHMO_{closed}$ were collected on a Rigaku RUH-3R generator equipped with an R-axis IV++ detector, while $CHMO_{open}$ was collected at beamline X6A of the National Synchrotron Light

(16) Alphand, V.; Furstoss, R. *Tetrahedron: Asymmetry* **1992**, *3*, 379–382.
(17) Malito, E.; Alfieri, A.; Fraaije, M. W.; Mattevi, A. *Proc. Natl. Acad. Sci. U.S.A.* **2004**, *101*, 13157–13162.
(18) Iwaki, H.; Hasegawa, Y.; Wang, S.; Kayser, M. M.; Lau, P. C. K. *Appl. Environ. Microbiol.* **2002**, *68*, 5671–5684.
(19) Iwaki, H.; Wang, S.; Grosse, S.; Bergeron, H.; Nagahashi, A.; Lertvorachon, J.; Yang, J.; Konishi, Y.; Hasegawa, Y.; Lau, P. C. K. *Appl. Environ. Microbiol.* **2006**, *72*, 2707–2720.

Table 1. Summary of Crystallographic Data[a]

	crystal form I ($CHMO_{open}$)	crystal form II ($CHMO_{closed}$)
space group	$P2_12_12_1$	$P2_12_12_1$
a, Å	64.3	62.5
b, Å	67.0	91.0
c, Å	136.0	100.4
resolution range, Å	20.0−2.2	50.0−2.3
completeness, %	99.4 (97.0)	99.9 (99.9)
redundancy	5.5 (3.4)	6.8 (6.7)
R_{merge}	0.08 (0.36)	0.10 (0.54)
R_{factor}/R_{free}	18.3/24.5	17.9/24.8
no. of reflections	27 243 (3788)	23 460 (3390)
no. of atoms	4364	4446
no. of protein atoms	4014	4166
no. of cofactor atoms	101	127
no. of solvent atoms	249	153
rms bond length, Å	0.017	0.021
rms bond angle, °	1.784	1.963

[a] Data in parentheses represent the outermost shell.

Source. Both data sets were collected under standard cryogenic conditions and processed using the HKL2000 suite of programs[20] (Table 1).

Structure Determination and Refinement. The structure of $CHMO_{open}$ was determined by molecular replacement using the program PHASER[21] and the coordinates of PAMO (PDB ID 1W4X) as the search model.[17] Upon identification of the appropriate rotation and translation matrix, the model was mutated using the program Modeller[22] to reflect the sequence of CHMO. This model was then subjected to multiple rounds of high-temperature simulated annealing refinement using the program CNS.[23] Upon convergence of the crystallographic *R*-factors, refinement was switched over to REFMAC5 and included positional and *B*-factor refinement, with subsequent TLS refinement being applied toward the end stage.[24] Manual model rebuilding was carried out iteratively during the course of refinement using the program PyMol.[25] Phasing of $CHMO_{closed}$ was achieved using the nearly completed structure of $CHMO_{open}$ and employed an analogous refinement strategy as the latter. Figures were prepared using the program PyMol.[25]

The atomic coordinates and structure factor amplitudes have been deposited in the Protein Data Bank, www.pdb.org (PDB ID codes 3GWD and 3GWF).

Results

Rhodococcus sp. strain HI-31 is a new environmental isolate, selected by growth on cyclohexanone as a sole source of carbon, and found to encode at least two CHMO-related sequences (*chnB1 and chnB2*) within a 17.1-kilobase pair sequenced region (DDBJ accession no. AB471785 and SI). The *chnB1* gene was cloned in *E. coli*, and the protein, henceforth designated simply as CHMO, was overproduced and purified. This enzyme is a stable, monomeric, 540 residue protein, displaying characteristic flavoprotein absorption maxima at 376 and 477 nm and a minimum at 405 nm, consistent with the observation that it contains 0.94 mol of FAD per mol of enzyme. In an unrooted phylogenetic analysis of known BVMOs and a selected list of genomic BVMO sequences (SI-Figure 5), CHMO is positioned in the same branch as the classical cyclohexanone monooxygenase from *Acinetobacter* sp. NCIMB9871 ($CHMO_{AC}$), sharing an overall 55% sequence identity (SI-Figure 6).

Substrate Profiling. Mirroring the sequence similarity, the regio- and enantiospecificity of this CHMO are also highly similar to those of $CHMO_{AC}$ (SI-Table 2); however, it appears that CHMO has a broader substrate spectrum than $CHMO_{AC}$. The former readily accepted 4-*tert*-butylcyclohexanone (compound **7**) as a substrate with excellent enantioselectivity (>99% ee), compared to the poor activity obtained by $CHMO_{AC}$. A similar trend was observed for compounds **8**−**13**. Finally, CHMO also showed very good activity with the decalone-type bicyclic ketones (**14**−**16**). It is noteworthy that 2-tetralone was selectively oxidized to only one isomer.

Overall Structure. Crystal structures of CHMO in complex with FAD and $NADP^+$ were determined in two different crystal forms to a resolution of 2.3 and 2.2 Å (Table 1). Nearly all of the polypeptide chain could be modeled in both crystal forms, except for the first and last 5−7 residues. In crystal form I ($CHMO_{open}$), residues 487−504 were also not modeled due to the absence of appropriate density. This segment presumably forms an unstructured loop. In both crystal forms, well-defined density was observed for the FAD and $NADP^+$ cofactors. Furthermore, in crystal form II ($CHMO_{closed}$), electron density corresponding to the nicotinamide half of a second $NADP^+$ molecule involved in stacking interactions with W50 was observed. The presence of this second, partially ordered $NADP^+$ does not have any known biological function.

The three-dimensional architecture of CHMO, which mirrors that of PAMO, is highly modular in nature and can be separated into three domains and numerous loops (Figure 1). The FAD binding domain is composed of the first 140 N-terminal residues, supplemented with residues 387−540 from the C-terminus. The NADP binding domain is composed of discontinuous segments 152−208 and 335−380. Inserted within the sequence of the NADP domain and connected by residues 209−223 and 322−334 is an entirely helical domain comprised of residues 224−322. This domain serves as a modulating region between the two dinucleotide binding domains and also provides crucial residues that make up the substrate binding pocket.

Connecting the FAD and NADP domains are two unstructured loop segments made up from residues 144−151 and residues 381−386. It is noteworthy that the linkers are very well defined in the $CHMO_{closed}$ crystal form, whereas these residues generally have higher *B*-factors and have less defined density in $CHMO_{open}$, suggesting some degree of conformational flexibility. The FAD cofactor is buried deep within the FAD domain, consistent with the observation that this cofactor does not dissociate from the enzyme, while the $NADP^+$ is sandwiched between the Rossmann fold of the NADP domain and a loop region of the FAD domain. In both crystal forms, a substrate binding site can be observed at the juxtaposition of the NADPH and FAD binding sites.

Domain Movements. Identification of two different $NADP^+$ cocrystallization conditions has allowed for the determination of two distinct structures that reveal significant differences. The two main variations between the $CHMO_{open}$ and $CHMO_{closed}$ crystal forms are in the relative domain orientations and an order/disorder transition of loop 487−504. These differences perpetuate alternate cofactor binding modes and effect significant changes in the substrate binding pocket.

(20) Otwinowski, Z.; Minor, W. *Methods in Enzymology*; Academic Press: New York, 1997; Vol. 276, pp 307−326.
(21) McCoy, A. J.; Grosse-Kunstleve, R. W.; Storoni, L. C.; Read, R. J. *Acta Crystallogr. D: Biol. Crystallogr.* **2005**, *61*, 458–464.
(22) Eswar, N.; Eramian, D.; Webb, B.; Shen, M. Y.; Sali, A. *Methods Mol. Biol.* **2008**, *426*, 145–159.
(23) Brunger, A. T.; Adams, P. D.; Clore, G. M.; DeLano, W. L.; Gros, P. *Acta Crystallogr. D: Biol. Crystallogr.* **1998**, *54*, 905–921.
(24) Murshudov, G. N.; Vagin, A. A.; Dodson, E. J. *Acta Crystallogr. D: Biol. Crystallogr.* **1997**, *53*, 240–255.
(25) DeLano, W. L. *The PyMOL molecular graphics system*; DeLano Scientific: Palo Alto, CA, 2002.

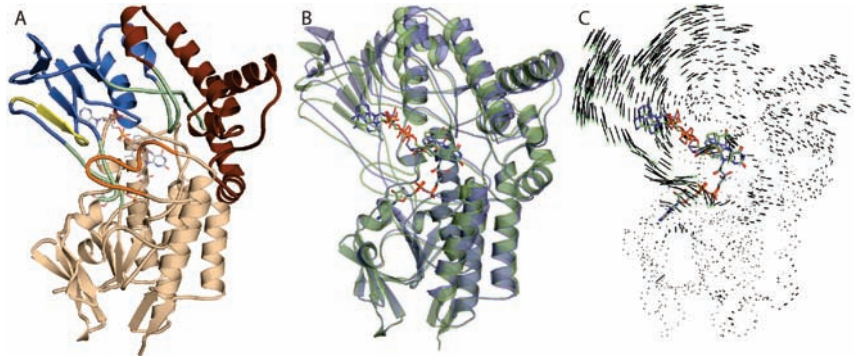

Figure 1. Color-coded cartoon representation of overall domain structure of CHMO and examination of conformational changes: (A) wheat, FAD domain; dark blue, NADP domain; light green, linker regions; brown, helical domain; orange, mobile loop region; and yellow, BVMO signature motif. (B) FAD domain-anchored structural superposition of $CHMO_{open}$ (blue) and $CHMO_{closed}$ (green). (C) Equivalent atoms vector diagram illustrating changes in relative backbone atoms positions between $CHMO_{open}$ and $CHMO_{closed}$ (dark blue and purple regions from panel a). Notable is the large rotation of the NADP domain with a concurrent similar albeit less pronounced movement of the helical domain.

Using the core FAD binding residues as an anchor (backbone rms 0.3 Å), comparison of the two structures reveals a 5° rotation of the NADP domain centered at the active-site cavity, which translates to an over ~5 Å backbone shift for residues distal to the axis of rotation (Figure 1). Displaying a similar albeit less prominent movement, the helical domain returns an average backbone rotation of ~3°, resulting in shifts in the order of 2 Å for distal residues. The movement of both the NADP domain and the helical substrate domain is made possible by the flexing of the four connector loops.

Another important difference that can be observed between $CHMO_{open}$ and $CHMO_{closed}$ is in the conformation of residues 487−504. In $CHMO_{open}$, this loop is not visible and likely adopts a flexible, solvent-exposed conformation similar to that observed in the structure of PAMO. This is in sharp contrast to the $CHMO_{closed}$ structure, where this loop folds back onto itself, internalizing the center portion of this segment (residues 490−493).

$NADP^+$ Binding. In both the $CHMO_{open}$ and $CHMO_{closed}$ crystal forms, the $NADP^+$ cofactor adopts an extended conformation, with its diphosphate backbone forming hydrogen bond interactions with a GXXGXG motif (residues 182−187). Further stabilization of the cofactor is afforded through interactions between the 2′ phosphate of $NADP^+$ and OG of T210 and NE of R209. The guanidinium moiety of R209 is also involved in stacking interactions with the adenine base. In both crystal structures, the cofactor is oriented in such a manner that the B-face of the nicotinamide ring is facing the isoalloxazine ring, suggesting *pro*-S hydride transfer during flavin reduction (Figure 2), which differs from what has been suggested for PAMO on the basis of kinetic studies.[26] The presence, however, of similarly oriented cofactors in two independently determined crystal forms as well as the observation of the same orientation in multiple FMO structures suggests that this manner of cofactor orientation is likely the more frequently observed, biologically relevant mode of binding.[27,28]

The similar yet distinct movements of the NADP and helical domains serve to modulate large shifts while at the same time permitting more subtle changes in the active-site binding pocket.

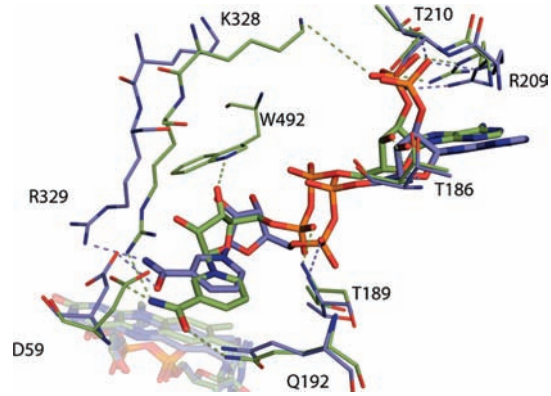

Figure 2. Comparison of $CHMO_{open}$ (blue) and $CHMO_{closed}$ (green) $NADP^+$ binding modes. The cofactor binds to the NADP domain through interactions with T210, R209, T186, T189, and Q192, which are the same in both the open and closed conformations. By contrast, large shifts can be noted in residues D59, K328, R329, and W492 between the conformations leading to the "push" configuration observed in $CHMO_{closed}$.

For instance, between the two structures, there is an average 1.7 Å backbone shift for residues 326−330. The two residues most affected by this shift are K328 and R329. The strictly conserved K328 has previously been implicated in NADPH vs NADH selectivity;[29] however, in $CHMO_{open}$ it does not appear to interact with this cofactor, given a distance of over 10 Å between the closest possible H-bonding partners. Alternatively, in $CHMO_{closed}$, a 4.2 Å shift and concurrent rotation result in decreased distance between NZ K328 and a phosphoryl oxygen, suggesting a possible indirect interaction between these atoms. Similarly, R329, which makes H-bonding contact with the amide nitrogen of $NADP^+$ in both crystal forms, undergoes an overall 2.7 Å shift. This results in this residue moving closer toward the interior of the enzyme, effecting concurrent movements in the cofactor $NADP^+$.

In $CHMO_{open}$, the nicotinamide base is held in place through an H-bond with D59 and stacking interactions with the xylene portion of the FAD isoalloxazine ring system. Contrasting this, in $CHMO_{closed}$, flexing of the phosphate backbone brought about by an interaction between the 2′-hydroxyl of the nicotinamide ribose and W492 as well as R329 and nicotinamide amide nitrogen results in a sliding of the nicotinamide head, allowing

(26) Torres Pazmiño, D. E.; Baas, B. J.; Janssen, D. B.; Fraaije, M. W. *Biochemistry* **2008**, *47*, 4082–4093.
(27) Alfieri, A.; Malito, E.; Orru, R.; Fraaije, M. W.; Mattevi, A. *Proc. Natl. Acad. Sci. U.S.A.* **2008**, *105*, 6572–6577.
(28) Eswaramoorthy, S.; Bonanno, J. B.; Burley, S. K.; Swaminathan, S. *Proc. Natl. Acad. Sci. U.S.A.* **2006**, *103*, 9832–9837.
(29) Kamerbeek, N. M.; Fraaije, M. W.; Janssen, D. B. *Eur. J. Biochem.* **2004**, *271*, 2107–2116.

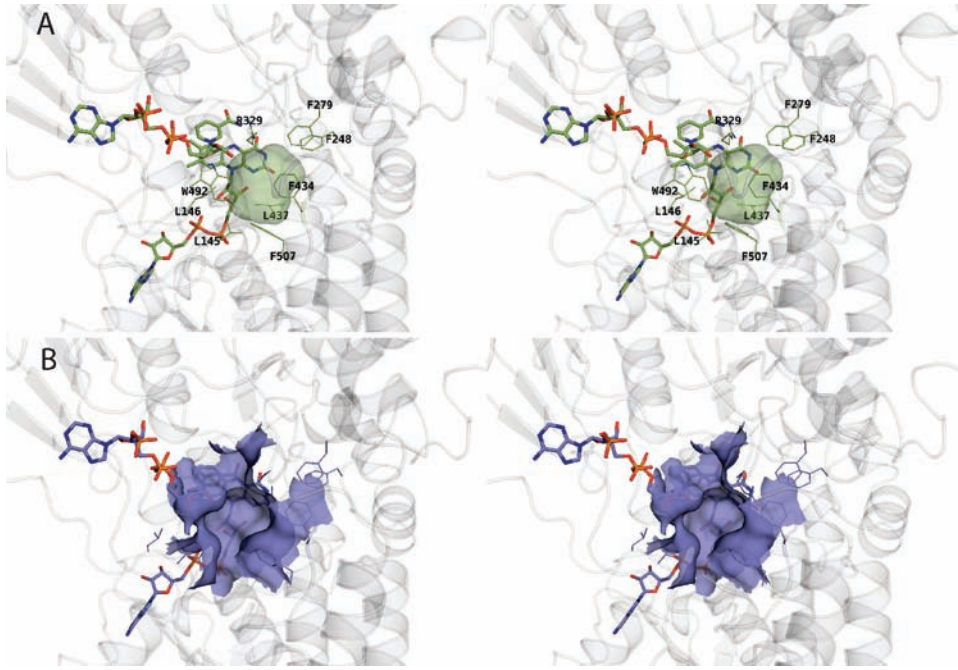

Figure 3. Comparison of active-site pockets observed in $CHMO_{closed}$ and $CHMO_{open}$. (A) Stereodiagram showing an enclosed cavity of ~150 $Å^3$ in $CHMO_{closed}$ that is formed by residues with a predominately hydrophobic character. (B) In $CHMO_{open}$, the same pocket is enlarged and surface accessible due to the movement of the mobile loop formed by residues 487−504.

for cofactor−protein interactions at Q192 and D59. Intriguingly, W492 is a strictly conserved residue among all known CHMOs and is located on a mobile loop formed from residues 487−504. To examine the relevance of this interaction, we mutated W492 to Ala, which resulted in a protein with only 14% of the original activity using cyclohexanone as substrate (0.85 U/mg compared to 6.0 U/mg of specific activity for CHMO).

Focusing on the $NADP^+$ and using the FAD domain as an anchor, the rmsd of the $NADP^+$ from $CHMO_{open}$ to $CHMO_{closed}$ is ~2 Å. The largest movement is a result of rotations in the diphosphate backbone that effect a lateral translation of the nicotinamide head (Figure 2). Consequently, the nucleotide slides parallel to the FAD xylene moiety. In both the $CHMO_{open}$ and $CHMO_{closed}$ conformations, the distance between $NADP^+$-NC4 and FAD-NC6 is ~3.3 Å, albeit shifted by 45°. It is noted that neither conformation appears to be conducive to flavin reduction through hydride transfer between the nicotinamide and isolloaxazine rings.

Substrate Binding Pocket. A substrate binding site can be identified in close proximity to the flavin ring in $CHMO_{closed}$. This enclosed cavity is defined by residues 145−146, 248, 279, 329, 434−435, 437, 492, and 507, as well as the FAD and $NADP^+$, and has a calculated volume of ~150 $Å^3$.[30] A similar pocket is also present in $CHMO_{open}$, but it is less defined, is not enclosed, and is solvent accessible (Figure 3). While the observed $CHMO_{closed}$ substrate binding pocket should be able to hold the primary substrate, cyclohexanone (SI-Figure 7), it does not appear large enough to hold some of the larger substrates that CHMO can oxygenate (SI-Table 2). However, at least one wall of the active site is formed by elements from mobile loop 487−504, allowing for some degree of plasticity and accommodation with respect to substrate binding.

Discussion

We present here the first structures of a CHMO and the first structures of a BVMO in the presence of both FAD and $NADP^+$. Although this protein originated from a *Rhodococcus* species, its sequence in a phylogenetic analysis is found to cluster with those of *Acinetobacter, Brachymonas*, and *Xanthobacter* CHMOs, making it representative of this family of BVMOs (SI-Figure 5).[31] The dual cofactor bound structures clarify how this protein adopts multiple conformations during catalysis, highlighting the diverse roles played by the nicotinamide cofactor during the enzymatic process and the effect this has on changing the size and accessibility of the substrate binding pocket. Because of this, we can now precisely identify mobile portions of the enzyme that can be used to predict other catalytically relevant conformations.

$NADP^+$ Binding. While the backbone contacts with the $NADP^+$ are essentially identical in both crystal structures, the relative orientation of the NADP domain results in a cofactor that undergoes a significant lateral translation between the two crystal forms. Examination of the $CHMO_{open}$ structure reveals that the nicotinamide and isoalloxazine ring systems are parallel to each other, with a closest distance of 3.4 Å between C4 of the nicotinamide and C6 of the xylene moiety. Despite such a close interaction, it is unlikely that this conformation is the mode of binding responsible for the NADPH-dependent reduction of the flavin, as hydride transfer would normally be expected to occur between C4 of the nicotinamide and N5 of the flavin. Contrasting this, the $CHMO_{closed}$ structure is in a somewhat unique and surprising conformation. Rotation of the NADP domain results in a lateral translation of the cofactor, pushing

(30) Kleywegt, G. J.; Jones, T. A. *Acta Crystallogr. D: Biol. Crystallogr.* **1994**, *50*, 178–185.

(31) Rial, D.; Cernuchova, P.; van Bielen, J.; Mihovilovic, M. *J. Mol. Catal. B: Enzymatic* **2008**, *50*, 61–68.

the nicotinamide head into a shallow pocket located between residues 55 and 59. In this conformation the amide nitrogen is within hydrogen-bonding distance of the flavin N5 and O4. More importantly, however, this positively charged moiety is also available for the stabilization of the requisite flavin-C4A peroxide moiety (Figure 2). This negative charge-stabilizing role is analogous to that carried out by $NADP^+$ in FMO, with the two enzymes adopting similar conformations with respect to the orientation of the two cofactors.[27]

Immediately adjacent to the active site, K328 has been implicated in cofactor binding and NADPH vs NADH selectivity.[29] However, in neither $CHMO_{closed}$ nor $CHMO_{open}$ does the K328 appear to interact directly with the cofactor. This lack of an observed interaction despite biochemical evidence to the contrary suggests that there exists at least one more NADP(H)-bound conformation involved in flavin reduction. It is also interesting to note that for K328 to interact with the phosphate group would require only a small rotation of the NADP domain. This would also have the effect of repositioning the nicotinamide head laterally so that it would be more accessible for the expected hydride transfer between C4 of the NADPH and N5 of the FAD.

Previously, it had been suggested that the strictly conserved R329 plays an important role in catalysis, with the equivalent R337 having been observed in multiple conformations in the PAMO structure. These "in" and "out" conformations were speculated to be important in stabilization of the peroxyanion intermediate, as well as in shifting during catalysis to accommodate NADPH binding.[17] In $CHMO_{open}$, R329 occupies a conformation similar to the "out" structure. In this position, there is a distance of 3.2 Å between NH of R329 and the amide nitrogen of $NADP^+$. This interaction may effect the relatively tight binding of oxidized $NADP^+$ to the enzyme, post catalysis.

Contrasting the above similarities between the PAMO "out" and $CHMO_{open}$ structures, R329 appears to occupy a new locus in $CHMO_{closed}$. In this conformation, a slightly tighter interaction can be noted between NH and the $NADP^+$ at 2.9 Å; however, given the translation of the cofactor, R329 fills a position not previously observed. Unlike the PAMO structure, where the variations between "in" and "out" can be attributed to differences in rotomers, in $CHMO_{open}$ and $CHMO_{closed}$ R329 actually does not significantly change rotomeric conformations. Here, the large shift between the two structures is due to the flexing of loop 327−330 between the two structures, resulting in the pushing of the nicotinamide head by R329. For this reason, we have given this configuration the name "push". This movement is greatly facilitated by the closing of loop 487−504, which also serves to push $NADP^+$ deeper into the enzyme via interactions with W492. In this manner, R329 is now ideally situated to facilitate the reaction of molecular oxygen with reduced FAD and subsequently stabilize either the peroxyflavin or Criegee intermediates (Figure 2 and SI-Figure 7).

Given the two different modes of $NADP^+$ binding, we speculate that these structures represent two specific time points in a very dynamic catalytic cycle, as indicated by spectroscopic data.[15] Our results suggest that the $CHMO_{closed}$ structure mimics the conformation of the enzyme in the post flavin reduction (substrate binding) state, $E{\cdot}FADH^-{\cdot}NADP^+$, and the two subsequent steps (Scheme 1). Given the buried positioning of the $NADP^+$, this conformer is ideal for stabilization of the Criegee intermediate. Complementing this, the $CHMO_{open}$ structure likely represents the final step in the catalytic cycle, namely $NADP^+$ release ($E{\cdot}FADH^-{\cdot}NADP^+$ in Scheme 1).

Substrate Binding Site. Despite having the same overall fold, there are two important exceptions to the structural homology observed between CHMO and PAMO. The first is the Gly-Phe dipeptide insert in CHMO at positions 278−279, which results in a slight bulging of the loop connecting helix 262−275 and helix 281−285 (CHMO numbering). The second main structural deviation is between residues 433 and 434, where PAMO has a two-residue insertion. Both of these inserts are located in the $CHMO_{closed}$ substrate binding site and are undoubtedly responsible for the difference in substrate specificity observed in PAMO.[32] Another intriguing aspect of substrate specificity is the effect loop 487−504 plays in completing the active-site pocket. In $CHMO_{open}$, this loop is not visible and likely forms an unstructured loop similar to that found in PAMO. Alternatively, in $CHMO_{closed}$, this loop forms part of the closed active-site pocket, permitting interactions between W492 and the $NADP^+$ ribose. Mutagenesis of this conserved residue to alanine resulted in a protein with reduced activity. The exact nature of the interaction between this loop and the substrate, and the role it has in substrate specificity, will require further structural characterization. The expanded substrate spectrum of CHMO compared to that of $CHMO_{AC}$ may be attributable to differences in this loop.

Role of the BVMO Signature Motif in Cofactor Binding. The presence of a FXGXXXHXXXWP motif has been shown to be an identifier of type I BVMOs.[33] In the structure of the CHMO, this signature sequence is located at the start of the NADP domain spanning residues 160−171. A similar motif has been observed in the structurally similar FMOs (FXGXXXHXXX(Y/F)).[5] It has been demonstrated that this segment plays an essential role in cofactor binding and catalysis in that mutations of the central histidine have dramatic effects on enzyme activity. Somewhat paradoxically, the localization of the motif far from the active site has made it difficult to ascribe a direct function in catalysis, and thus the role was assumed to be structural. Here, the presence of the multiple crystal structures permits us to gain more insight into the role of this critical segment.

Comparison of the CHMO, PAMO, and available FMO structures reveals that the strictly conserved aromatic ends of the motif adopt nearly identical conformations. That is to say, in all available structures, the terminal residues are buried deep within the NADP binding domain and serve as "sticky ends" that securely fix the signature motif to the NADP domain. The role of the central histidine, however, is more complex. Based on the PAMO structure, it appears that this residue is completely solvent exposed in the absence of $NADP^+$/H and does not appear to have any direct or indirect role in substrate binding.[17] In the $NADP^+$-bound crystal structure of CHMO, however, this critical residue is rotated inward such that the imidazole ring of the histidine forms a hydrogen bond to the backbone of one of the flexible linker segments (residues 381−386). In addition to linking the FAD and NADP domains, this same linker region is also important in positioning the $NADP^+$ through steric interactions. It thus appears that although the signature motif does not play a role in catalysis directly, it is important as an atomic switch that tightly coordinates multiple unconnected portions of the enzyme to allow for binding and precise positioning of the $NADP^+$/H (Figure 4). This structural modula-

(32) Clouthier, C. M.; Kayser, M. M.; Reetz, M. T. *J. Org. Chem.* **2006**, *71*, 8431–8437.
(33) Fraaije, M. W.; Kamerbeek, N. M.; van Berkel, W. J.; Janssen, D. B. *FEBS Lett.* **2002**, *518*, 43–47.

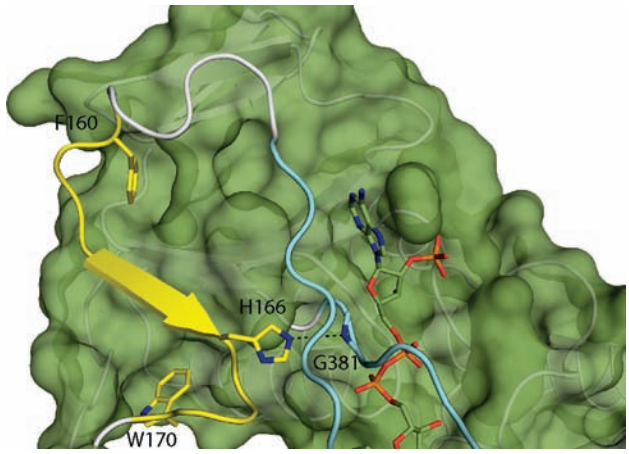

Figure 4. The BVMO signature sequence, shown here in yellow, is anchored at each end by F160 and W170, which interact with hydrophobic pockets in the NADP binding domain. In the middle of the motif, H166 is shown interacting with the backbone of G381, which is part of one of the linker segments shown in cyan that connect the FAD and NADP domains.

tion underscores the complexity and intricacy of the various rotations CHMO undergoes to facilitate catalysis.

Conclusion

Despite a tremendous body of literature developed for the study of CHMOs, until now, there has been no available crystal structure of a representative CHMO. Presently, the availability of multiple CHMO structures in complex with both FAD and $NADP^+$ provides snapshots of domain rotation and movements undertaken by this biocatalyst. These structures provide insight into how this enzyme can exploit the $NADP^+$/H cofactor for multiple purposes during the reaction cycle, as well as the critical role of the BVMO signature sequence. This work provides directions for further analysis and understanding of how the biocatalytic potential of these enzymes might be developed in the future.

Acknowledgment. The authors thank past and present members of the Berghuis and Lau laboratories for their assistance and suggestions. We also thank Marc Allaire for performing diffraction data collection at the National Synchrotron Light Source. The work at McGill was made possible through grants from the Natural Sciences and Engineering Research Council of Canada and Canadian Institute of Health Research awarded to A.M.B. A.M.B. holds a Canada Research Chair in Structural Biology. Work at Kansai University was supported in part by the Strategic Project to Support the Formation of Research Bases at Private Universities program. We thank Ping Xu for help in NMR analysis and G. Ottolina for helpful discussions.

Supporting Information Available: Cloning, overexpression, purification, mutagenesis, and substrate profiling of CHMO. This material is available free of charge via the Internet at http://pubs.acs.org.

JA9010578